STRUCTURE OF OSCILLATING VORTEX GENERATOR JETS

Ralph J. Volino and Douglas G. Bohl
Department of Mechanical Engineering
United States Naval Academy
Annapolis, Maryland 21402-5042, USA
volino@usna.edu

ABSTRACT

The suction side boundary layer of an airfoil passage was studied experimentally. The pressure gradient along the airfoil was typical of a low pressure turbine environment, and the Reynolds number, based on suction surface length and exit velocity, was 25,000. A row of oscillating vortex generator jets (VGJs), located at the pressure minimum on the suction side was used for flow control. The jets had no net mass flow and a dimensionless oscillation frequency, F^+, of 0.65. Velocity profiles were acquired with single and cross sensor hot-wire probes at multiple streamwise and spanwise positions downstream of the VGJs. Time averaged results showed that with the VGJs active, the boundary remained attached and essentially laminar, and was spanwise uniform. Without the VGJs the boundary layer separated and did not reattach. Phase averaged results showed that instantaneously the boundary layer was very non-uniform across the span. The outpulse of the jets generated turbulence and produced streamwise vortices, which brought high speed fluid into the near wall region and helped to keep the boundary layer attached. The vortices persisted to the trailing edge. A calmed region followed the jet pulsing events, and the calmed flow was characterized by a thin, spanwise uniform boundary layer that was resistant to separation. Phase averaged mean velocity, Reynolds stresses, and integral quantities are presented to illustrated the structure of the unsteady boundary layer.

INTRODUCTION

Vortex generator jets (VGJs) are used to control or prevent boundary layer separation. The jets, as described by Johnston and Nishi (1990), exit a surface from "small, skewed, and pitched holes" to create streamwise vortices similar to those created by solid vortex generators. Any jet will produce some turbulence, and the turbulent mixing will tend to bring high momentum fluid into the near wall region and inhibit separation. Streamwise vortices bring additional high momentum fluid into the near wall region. The most effective VGJs enter the boundary layer at a relatively shallow pitch angle relative to the wall and a high skew angle relative to the main flow. Compton and Johnston (1992) showed that the co-rotating vortices produced by VGJs are stronger and more effective for separation control than the counter-rotating vortices which form downstream of a normal jet.

The present use of VGJs is motivated by the need to control separation on the suction side of some low-pressure turbine (LPT) airfoils in aircraft engines. Airfoils are designed so that separation does not occur under takeoff conditions, where Reynolds numbers are relatively high. At altitude, however, the ambient density is lower, resulting in lower *Re* and separation problems. Passive devices such as solid vortex generators can be used to control separation, but they can increase aerodynamic losses at high *Re*. VGJs could be turned on only when needed, providing separation control at low *Re* with no harmful effects at high *Re*.

Most studies of VGJs have considered jets with steady flow (e.g. Johnston and Nishi, 1990 and Compton and Johnson, 1992), but a few have also considered pulsed jets. McManus et al. (1994) found that pulsed VGJs were more effective than steady jets in turbulent boundary layers. Bons et al. (2002) used pulsed jets to suppress separation in a laminar boundary layer under simulated LPT conditions. They used spanwise rows of VGJs on the suction surface of an airfoil, and found that a row near the suction surface pressure minimum was most effective. Reynolds numbers as low as 60,000 (based on suction surface length, L_s, and exit velocity, U_e) were considered. Bons et al. (2002) found that the pulsed jets were fully effective even when the dimensionless pulsing frequency, F^+, was as low as 0.1, where F^+ is a ratio of the transit time for flow between the VGJ hole and the trailing edge to the time interval between pulses. Ensemble averaged velocity profiles showed a long relaxation or "calmed" period following each jet pulse. During this calm period the boundary layer remained attached long after the turbulence generated by the pulse had moved downstream. Calmed regions have been observed following turbulent spots in transitional boundary layers (e.g. Gostelow et al., 1997). The mean velocity profiles in the calmed region gradually relax from a turbulent shape to a laminar (and in some cases separated) profile shape. The calmed boundary layer is very resistant to separation, much like a turbulent boundary layer, but it is very laminar-like in terms of its fluctuation levels and low losses. The pulsed jets were more effective than steady jets, even with pulsed jet duty cycles as low as 1%. This was believed to indicate that the starting vortex formed at the beginning of each pulse was responsible for most of the flow control with pulsed jets.

Volino (2003) considered oscillating jets with no net mass flow under conditions similar to those of Bons et al. (2002), but at a lower Reynolds number of 25,000. In uncontrolled flow, the laminar boundary layer separated and did not reattach. With the jets operating at a pulsing frequency F^+=0.65, the separation was effectively eliminated. The jets produced turbulent and calmed regions which kept the boundary layer attached. The leading and trailing edge celerities of the turbulent and calmed regions matched those expected for a turbulent spot. Following the calmed region, the boundary layer did separate, but the separation bubble was only present for a small fraction of the jet pulsing cycle, and it remained very small and thin. In fact, the boundary layer remained thin, laminar and attached along the entire airfoil over most of the cycle.

While pulsed and oscillating VGJs have been shown effective in a few studies, information about their structure is limited. Bons et al. (2002) and Volino (2003) provide data only at a single spanwise position. Johari and Rixon (2003) studied a single pulsed VGJ in a zero pressure gradient turbulent boundary layer using particle image velocimetry. They provide documentation of the location, vorticity and circulation of the streamwise vortices induced by the VGJ. More information is needed in cases with adverse pressure gradients, laminar flow and multiple VGJs. Also, quantities such as turbulence statistics and boundary layer integral quantities should be documented at multiple spanwise locations. It is not clear at present whether the turbulent and calmed flow produced by the VGJs is sufficient to prevent separation or whether the streamwise vortices are necessary. If the turbulence alone is sufficient, then simpler normal jets might suffice. The persistence or dissipation of the vortices in the streamwise direction is also unclear. The spanwise uniformity of the flow should be studied, as it is not certain that the vortices suppress separation across the entire span. The present study addresses these issues.

EXPERIMENTS

The experimental facility and measurements are described in detail by Volino (2003). Briefly, air enters a low speed wind tunnel through blowers and passes through a honeycomb, screens, settling chambers, and a contraction before entering the test section. At the exit of the contraction, the mean velocity is uniform to within 1%. The freestream unsteadiness is 0.5%±0.05%. Most of this is streamwise unsteadiness at frequencies below 20 Hz. The actual freestream turbulence intensity (as indicated by the cross-stream and spanwise components) is about 0.2%.

The test section follows the contraction and consists of the passage between two airfoils, as shown in Fig. 1. A large span to chord ratio of 4.3 insures nominally two-dimensional flow at the midspan of the airfoils. Just upstream of each airfoil are bleed flaps, which allow air to escape from the passage. The flaps, the inlet flow angle, and a tailboard on the pressure side of the passage are adjusted so that the leading edge flows and pressure gradient along the airfoils match those in a multi-airfoil cascade representation of a typical LPT.

The oscillating VGJs were produced from a plenum which extended along the span at about mid-chord within the suction side airfoil, as shown in Fig. 2. A loudspeaker was sealed to the wide end of a funnel, and the funnel was inserted into the plenum at one end of the airfoil. The speaker was powered by an audio amplifier, which was in turn driven with a sine wave by a function generator. Holes for the VGJs were drilled through the suction surface into the plenum in a spanwise line at the pressure minimum, s/L_s=0.514, where s is the distance from the leading edge along the suction surface and L_s=229

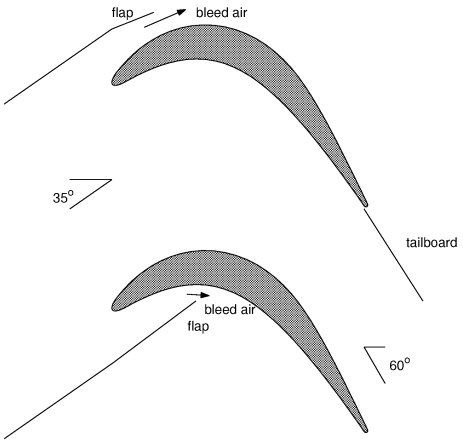

Fig. 1 Schematic of the test section

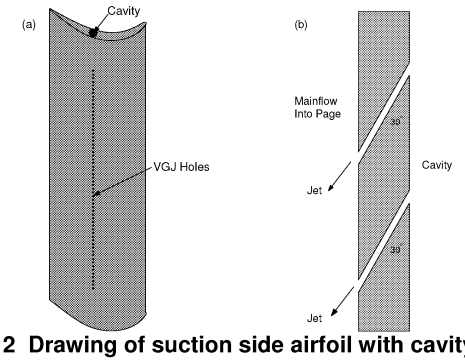

Fig. 2 Drawing of suction side airfoil with cavity and VGJs: (a) full airfoil, (b) cross section ofVGJ holes

mm. The hole diameter is $0.0035L_s$ and the spacing, P, is $0.037L_s$. The holes were drilled at a 90 degree skew angle with respect to the main flow and a 30 degree pitch with respect to the surface. The function generator and amplifier were set to produce jets with maximum velocity 5 times the local freestream velocity and dimensionless frequency F^+=0.65. Just upstream of the jets, the momentum thickness Reynolds number Re_θ=62, and the boundary layer thickness was 1.1 mm ($0.0048L_s$). The $Re=U_eL_s/\nu$ was 25,000.

Measurements consisted of velocity profiles acquired using hot-wire anemometry at five streamwise locations between the VGJ holes and the trailing edge. At each streamwise location, profiles were acquired at five spanwise positions. As in Volino (2003), a single-sensor probe was traversed from the wall to the freesteam, providing streamwise velocity data, from which boundary layer thicknesses and local skin friction coefficients, c_f, were computed (based on sublayer velocities). At the same streamwise and spanwise locations, a cross-wire probe was traversed from y=1mm from the wall to the freestream. At each measurement point, data were acquired for 26 s at a 20 kHz sampling rate. Details are available in Volino (2003).

Both time and phase averaged results are presented below. The velocity data were phase averaged at 24 evenly spaced increments around the jet pulsing cycle. At each increment, data were averaged over 1/180th of the cycle. For each 26 second data trace, this results in roughly 3000 data points to average for each ensemble. Uncertainties are 3% in the mean velocity, 10% in the momentum thickness, 8% in the shape factor and skin friction coefficient, and 10% in the Reynolds stresses. Further details are available in Volino (2003).

RESULTS

Figure 3 provides an example of the time averaged mean streamwise velocity, U, and time averaged turbulence statistics from the stations at s/L_s=0.78. Profiles are shown for the 5 spanwise measurement locations, with z/P=0 directly downstream of a VGJ hole, and z/P=1 directly downstream of the adjacent hole. All velocities and turbulence quantities in the figures are normalized using U_e. There is some spanwise variation in the rms u' profiles, although all have the same general double-peak shape. The U/U_e profile is essentially uniform across the span. The mean streamwise velocity profiles show that the boundary layer is attached, so the flow control is effective everywhere between the jets. Figure 4 shows the time averaged shape factor, $H=\delta^*/\theta$, and Re_θ at all locations. Again, there is little variation across the span. The shape factor rises at first, indicating a tendency toward separation, but it remains between 2 and 2.6, indicating an attached laminar boundary layer. As the time averaged flow is essentially spanwise uniform, further details can be obtained from the time averaged results presented in Volino (2003) for a single spanwise position.

Although the time averaged results are spanwise uniform, instantaneously there is considerable non-uniformity when the jet disturbance passes. The time average is simply dominated by the period between disturbances, which is uniform. The remainder of the present paper focuses on phase averaged results. Figure 5 shows contour plots of the mean streamwise velocity in the y-z plane at streamwise locations s/L_s=0.61 (Figs. 3a,b) and 0.94 (Figs. 3c,d). The data shown at $0<z/P<1$ are repeated at $1<z/P<2$ and $2<z/P<3$ to illustrate the periodic nature across the span. Plots are shown for the period between jet disturbances (Figs. 3a,c) and while the disturbance is present (Figs. 3b,d). In the figure captions, t is the time from the start of the cycle (roughly when the outflow begins at the VGJ hole) and T is the cycle period. Between disturbances the boundary layer is spanwise uniform and thin. The streamwise boundary layer growth can also be observed. In the presence of the disturbance there is a clear variation across the span, and it persists to the trailing edge. Figure 6 shows the data from Fig. 5 as velocity profiles. Comparison of Figs. 6b and 6d shows that the spanwise variation is clearly stronger at the upstream station.

Figure 7 shows the jet induced change in the mean wall-normal velocity, ΔV. That is, the mean V fields corresponding to the planes and phases of Figs. 5a and 5c were subtracted from the mean V fields corresponding to Figs. 5b and 5d respectively. Upwash ($\Delta V>0$) and downwash ($\Delta V<0$) regions are clear. The upwash corresponds to the region of low streamwise velocity in Fig. 5, as low speed fluid is pulled away from the wall. The downwash correspond to the region of high streamwise velocity, where higher speed fluid is brought closer to the wall. The vortices and their associated mixing persist to the trailing edge.

The behavior of the boundary layer over the course of a jet pulsing cycle is shown in Fig. 8, which shows contours of the rms fluctuating streamwise velocity u' in a plane at s/L_s=0.78. Results are shown for evenly spaced phases over part of a full jet pulsing cycle. In the phase shown in Fig. 8a, the boundary layer is between disturbances, and u' is essentially zero. In Fig. 8b, the disturbance is just beginning to arrive, and u' levels start to increase at $y/P\approx1$. The variation across the span is clear. At the next phase shown (Fig. 8c), the magnitude of u' has increased, with a peak still at $y/P\approx1$ and a second peak near the wall. The double peaks agree with the time averaged profiles of Fig. 3b. The next three phases of Fig. 8 (Figs. 8d-f) show u' decreasing in the outer part of the boundary layer and remaining high near the wall. In the remaining three phases

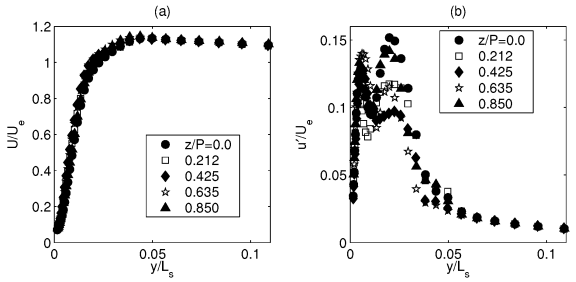

Fig. 3 Time averaged U/U$_e$ and rms u′/U$_e$ at s/L$_s$=0.78

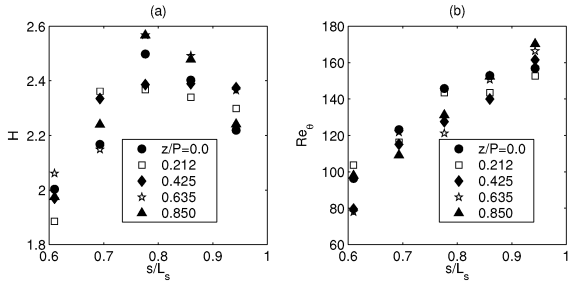

Fig. 4 Time averaged a) H and b) Re$_\theta$

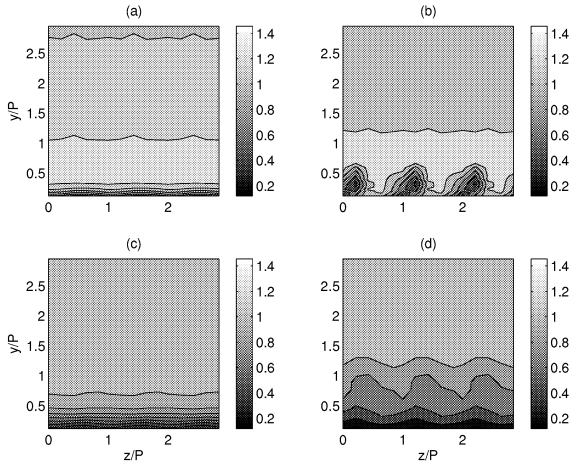

Fig. 5 Phase averaged U/U$_e$ at a) t/T=0.04, s/L$_s$=0.61; b) t/T=0.54, s/L$_s$=0.61; c) t/T=0.71, s/L$_s$=0.94; d) t/T=0.08, s/L$_s$=0.94

(Figs. 8g-i), the u' level drops back to the undisturbed value near zero. For the rest of the cycle (not shown) the u' level remains low, as in Fig. 8a. The behavior shown in Fig. 8 is typical of all streamwise locations. The disturbance first appears near the edge of the undisturbed boundary layer and then moves into the near wall region. The disturbance level then begins to drop, first in the outer part of the boundary layer and then near the wall. For a significant part of the cycle the boundary layer is undisturbed. The fraction of the time that the boundary layer is disturbed increases in the streamwise direction. This occurs, as shown in more detail for a single spanwise position in Volino (2003), because the leading edge of the disturbance travels faster than the trailing edge.

Figure 9 shows the Reynolds shear stress, $u'v'$ at the same location and phases as in Fig. 8. The disturbance has not arrived yet in Fig. 9a, and $u'v'$ is essentially zero everywhere. By the third phase shown (Fig. 9c), negative valued peaks appear at $y/P\approx1$ and very near the wall. The negative sign is

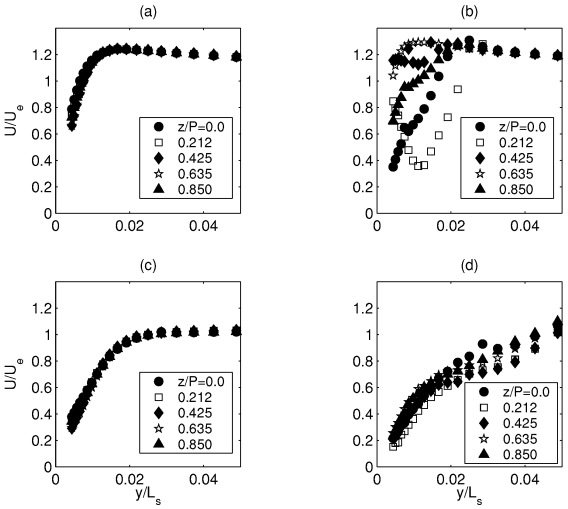

Fig. 6 Phase averaged U/U_e profiles at a) t/T=0.04, s/L_s=0.61; b) t/T=0.54, s/L_s=0.61; c) t/T=0.71, s/L_s=0.94; d) t/T=0.08, s/L_s=0.94

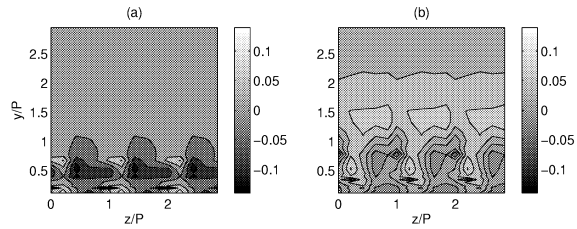

Fig. 7 Phase averaged $\Delta V/U_e$ at a) t/T=0.54, s/L_s=0.61; b) t/T=0.08, s/L_s=0.94

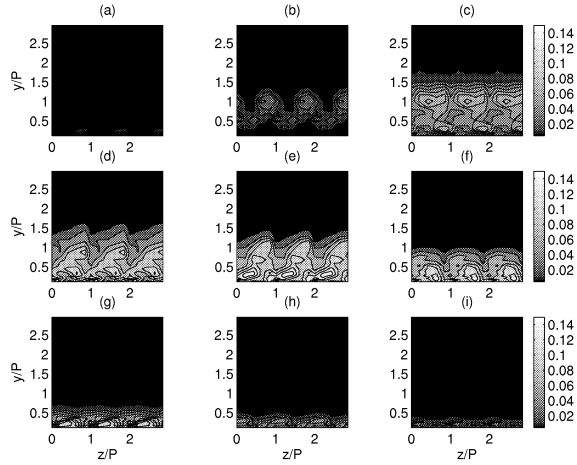

Fig. 8 Phase averaged u'/U_e at s/L_s=0.78, t/T= a) 0.50, b) 0.58, c) 0.67, d) 0.75, e) 0.83, f) 0.92, g) 0.0, h) 0.08, i) 0.16

expected for $u'v'$ and the locations agree with the peak locations in u' shown in Fig. 8c. There is also a small positive peak at $y/P \approx 0.5$, centered between the negative peaks. The data from Fig. 9c are shown as profiles in Fig. 10 for a better quantitative comparison. The positive peak is clear at z/P=0.212, and the two negative peaks are largest at z/P=0 and z/P=0.425. Negative $u'v'$ is typical of most boundary layers since the mean streamwise velocity generally increases with distance from the wall. If turbulence causes slow fluid to

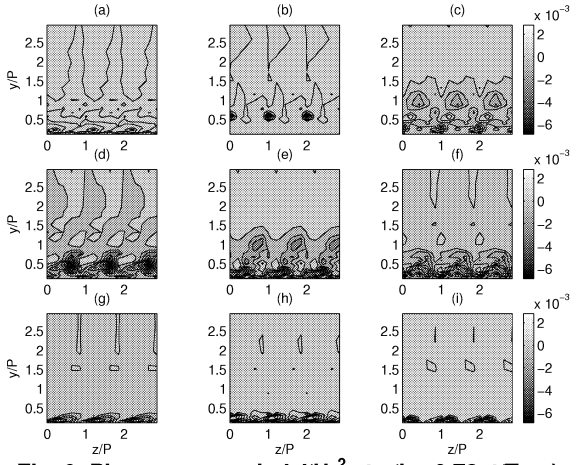

Fig. 9 Phase averaged $u'v'/U_e^2$ at s/L_s=0.78, t/T= a) 0.50, b) 0.58, c) 0.67, d) 0.75, e) 0.83, f) 0.92, g) 0.0, h) 0.08, i) 0.16

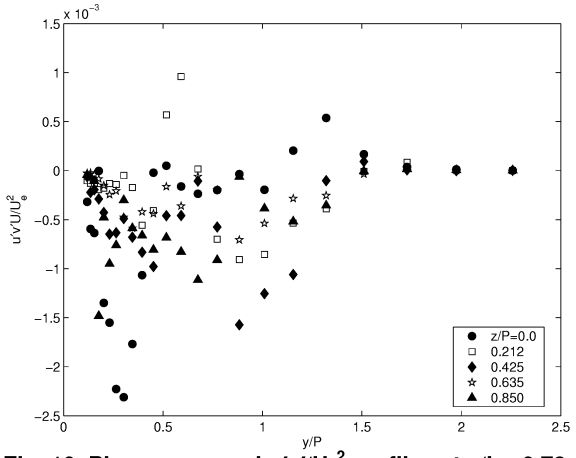

Fig. 10 Phase averaged $u'v'/U_e^2$ profiles at s/L_s=0.78, t/T=0.67

move away from the wall, v' will be positive and u' will be negative, resulting in negative $u'v'$. If higher speed fluid moves toward the wall, the result is again negative $u'v'$. In the present case, however, the streamwise vortices created by the VGJs cause instantaneously negative local streamwise velocity gradients, as shown in Fig. 6b. This causes the local positive $u'v'$ in Fig. 9c. In Fig. 9d, the negative $u'v'$ reaches its highest magnitude. In Figs. 9e-g, the $u'v'$ magnitude gradually descreases, and at the last two phases shown (Figs. 9h-i), $u'v'$ is near zero. The nonzero $u'v'$ caused by the VGJs is indicative of the turbulent mixing which helps to keep the boundary layer attached. The near zero $u'v'$ a for most of the jet pulsing cycle is indicative of a laminar boundary layer, and helps explain the laminar like time averaged velocity profiles of Fig. 3a. Comparing Figs. 8g-i and Figs. 9g-i, $u'v'$ returns to zero before u'. Volino (2003) also saw this faster return of $u'v'$ to zero and noted that the calmed region following the disturbance is characterized by some velocity fluctuations in u', but very little momentum transport.

For a different perspective on the boundary layer behavior, Fig. 11 shows the phase averaged u' results in an s-z plane at y=2 mm (y/L_s=0.0087, y/P=0.23). Three phases of the cycle are shown, and the convection of the disturbance along the surface and its three-dimensional nature are clear. In Fig. 11a, one disturbance is just leaving the trailing edge, while the next

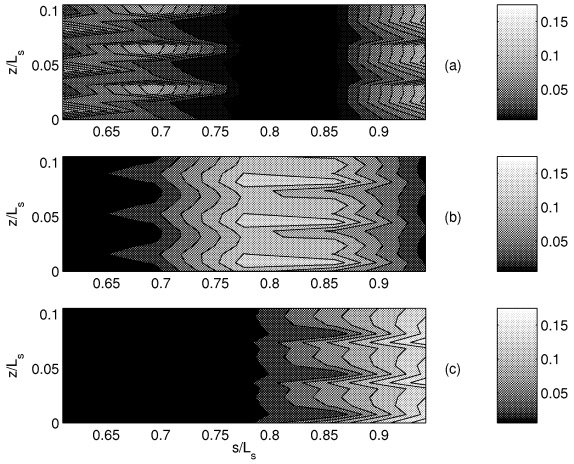

Fig. 11 Phase averaged u′/U$_e$ at y/Ls=0.0087 and a) t/T=0.54; b) t/T=0.88; c) t/T=0.21

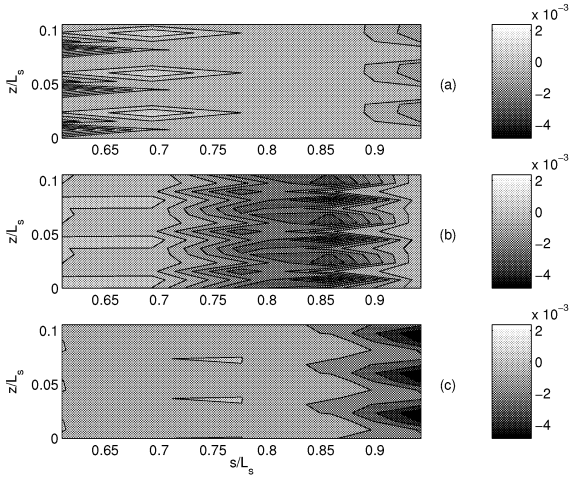

Fig. 12 Phase averaged u′v′/U$_e$ at y/Ls=0.0087 and a) t/T=0.54; b) t/T=0.88; c) t/T=0.21

disturbance is present at lower s/L_s. The second disturbance is then seen moving across the surface in Figs. 11b-c. Note that u' is near zero over for much of the cycle at all locations, indicating a laminar boundary layer. Figure 12 shows the Reynolds shear stress at the same locations and phases as in Fig. 11. Qualitatively, Figs. 11 and 12 are very similar. In Fig. 12a, regions of positive $u'v'$ are visible at s/L_s=0.7, as were also noted in Figs. 9c and 10. In other areas, $u'v'$ is negative. Over much of the cycle, the boundary layer is laminar and $u'v'$ is near zero.

Integral quantities were computed from the phase averaged streamwise velocity profiles. Figure 13 shows the local Re_θ at the same phases shown in Figs. 11 and 12. The VGJ disturbance causes a local thickening of the boundary layer, but in the absence of the disturbance θ is very low, even near the trailing edge. Figure 14 shows the shape factor, $H=\delta^*/\theta$, at the same phases. When the boundary layer is laminar and attached, H is between about 2 and 2.5. When it becomes turbulent, the value drops. If the boundary layer approaches separation, the shape factor increases significantly while the momentum thickness remains nearly constant. The result is a high shape factor. Comparing Figs. 11-14, H is highest between the VGJ disturbances. When the disturbance arrives at a location, H begins to drop, and it reaches its lowest value in the calmed period immediately after the disturbance has

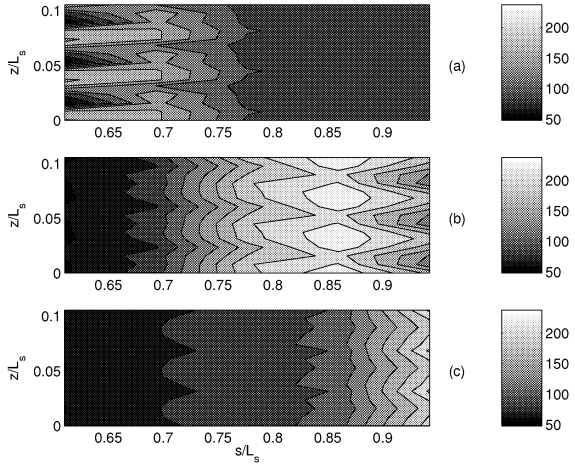

Fig. 13 Phase averaged Re$_\theta$ at y/Ls=0.0087 and a) t/T=0.54; b) t/T=0.88; c) t/T=0.21

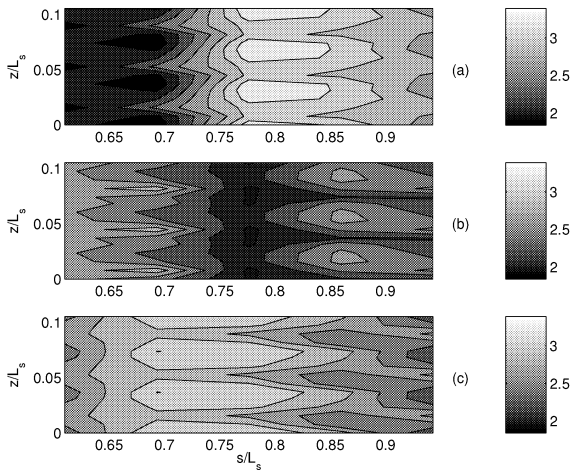

Fig. 14 Phase averaged shape factor, H, at y/Ls=0.0087 and a) t/T=0.54; b) t/T=0.88; c) t/T=0.21

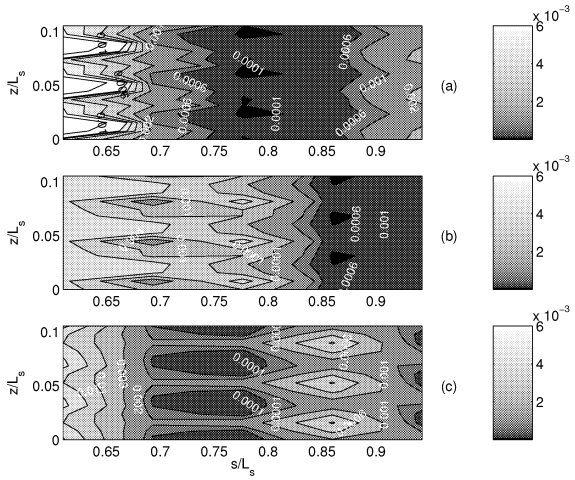

Fig. 15 Phase averaged c$_f$ at y/Ls=0.0087 and a) t/T=0.54; b) t/T=0.88; c) t/T=0.21

past. Hence, the disturbance keeps the boundary layer attached, and the effect persists into the calmed period. Following the calmed period, the boundary layer begins to relax toward its uncontrolled, separated state. Figure 15 shows the local skin friction coefficient at the same phases as Figs. 11-14. The black regions indicate c_f=0 and separated flow. When the jets begin their outward pulse, they induce high speed fluid into the near wall region, resulting in very high skin friction just downstream of the jet holes, as shown by the white regions in Fig. 15a. Between the turbulent regions the skin friction is very low, and the boundary layer momentarily separates at locations between s/L_s=0.7 and 0.9. The regions of zero or very low c_f in Fig. 15 are consistent with the regions of high H in Figs. 14. Figure 15b shows the boundary layer is separated at s/L_s=0.86, and Figs. 11b and 12b show that the VGJ disturbance is above this low c_f location. Fig. 13b shows that Re_θ is high at this location, while Fig. 14b shows that H is relatively high. The disturbance has arrived and begun to affect the outer part of the boundary layer, but it has not affected the near wall region yet, so the boundary layer remains separated. Slightly upstream at s/L_s=0.78 and the phase of Fig. 15b, the skin friction is high, the shape factor is low and the disturbance has just past. This is the calmed region following the disturbance, where the boundary layer has fully reattached.

CONCLUSIONS

The response of a boundary layer to a row of VGJs has been shown. The time averaged flow is spanwise uniform, but instantaneously the boundary layer is very three-dimensional. Streamwise vortices bring high speed fluid into the near wall region, suppressing separation. Evidence of the vortices persists to the trailing edge. The disturbance induced by the jets produces turbulence, but the boundary layer is thin and laminar between disturbances. The boundary layer separates at some locations, but the separation bubble remains thin and is only present for a small fraction of the VGJ cycle.

ACKNOWLEDGEMENTS

This work was sponsored by the NASA Glenn Research Center. The grant monitor was David Ashpis. Additional matching support was provided by the Office of Naval Research to the second author as a Naval Academy postdoctoral fellow.

REFERENCES

Bons, J.P., Sondergaard, R., and Rivir, R.B., 2002, "The Fluid Dynamics of LPT Blade Separation Control Using Pulsed Jets," *ASME J. Turbomachinery*, Vol. 124, pp. 77-85.

Compton, D.A., and Johnston, J.P., 1992, "Streamwise Vortex Production by Pitched and Skewed Jets in a Turbulent Boundary Layer," *AIAA J.*, Vol. 30, pp. 640-647.

Gostelow, J.P., Walker, G.J., Solomon, W.J., Hong, G., and Melwani, N., 1997, "Investigation of the Calmed Region Behind a Turbulent Spot," *ASME J. Turbomachinery*, Vol. 119, pp. 802-809.

Johnston, J.P., and Nishi, M., 1990, "Vortex Generator Jets. Means for Flow Separation Control," *AIAA J.*, Vol. 28, pp. 989-994.

Johari, H., and Rixon, G.S., 2003, "Effects of Pulsing on a Vortex Generator Jet," *AIAA J.*, Vol. 41, pp. 2309-2315.

McManus, K., Legner, H., and Davis, S., 1994, "Pulsed Vortex Generator Jets for Active Control of Flow Separation," AIAA Paper 94-2218.

Volino, R.J., 2003, "Separation Control on Low-Pressure Turbine Airfoils Using Synthetic Vortex Generator Jets," *ASME J. Turbomachinery*, Vol. 125, pp. 765-777.